The Journal of Laryngology & Otology (2015), ***129***, *1085–1090.*

doi:10.1017/S0022215115002480

MAIN ARTICLE

Curvature measurement of human bilateral cochleae

J-F YU[1,2], K-C LEE[2,3], Y-L WAN[4], Y-C PENG[5]

[1]*Graduate Institute of Medical Mechatronics, Chang Gung University, Taoyuan,* [2]*Taiouan Interdisciplinary Otolaryngology Laboratory, Chang Gung University, Taoyuan,* [3]*Department of Electrical Engineering, Chang Gung University, Taoyuan,* [4]*Department of Medical Imaging and Intervention, Chang Gung Memorial Hospital at Linkou, Institute for Radiological Research, College of Medicine, Chang Gung University, Taoyuan, Taiwan, and* [5]*Department of Prosthodontics, Chang Gung Memorial Hospital at Linkou, Taoyuan, Taiwan*

Abstract

Objective: This study aimed to characterise the geometry of the human bilateral spiral cochlea by measuring curvature and length.

Method: Eight subjects were recruited in this study. Magnetic resonance imaging was used to visualise the right and left cochlea. Visualisation of the cochlear spiral was enhanced by T2 weighting and further processing of the raw images. The spirals were divided into three segments: the basal turn, the middle turn and the apex turn. The length and curvature of each segment were non-invasively measured.

Results: The mean left and right cochlear lengths were 3.11 cm and 3.95 cm, respectively. The measured lengths of the cochlear spiral are consistent with data in the literature derived from anatomical dissections. Overall, the apex turn segment of the cochlea had the greatest degree of curvature ($p < 0.05$). The mean apex turn segment curvatures for left and right cochleae were 9.65 cm^{-1} and 10.09 cm^{-1}, respectively.

Conclusion: A detailed description of the cochlear spiral is provided, using measurements of curvature and length. These data will provide a valuable reference in the development of cochlear implantation procedures for minimising the potential damage during implantation.

Key words: Ear; Cochlea; Magnetic Resonance Imaging; Image Processing, Computer-Assisted

Introduction

The human cochlea is a small, spiral shaped structure with approximately two and a half turns.[1] Typically, artificial cochlear implant insertion involves electrode placement in the inner ear, which exerts force upon the inner wall of the scala tympani, in both the basal turn and apex turn regions. The insertion force during an electrode placement is composed of forward pressure from the insertion, accompanying frictional forces, electrode recoil forces, and adhesion forces between the electrode and the inner cochlea.[2] The main factors influencing force during electrode implantation are surgical technique and electrode design.[2] Variations in these factors, in addition to natural variations in cochlear spiral length in the patient population, result in a range of possible electrode insertion forces. In practice, however, the applied force during electrode insertion is most heavily dependent on surgical technique and expertise, with a high risk of damage to the cochlea.[3] In recent years, numerous protocols have been developed regarding electrode insertion force and contour path, in order to optimise electrode insertion and minimise damage to the cochlea.[4–8]

Prior research has applied three-dimensional (3D) helicon-spiral modelling,[9] geometry modelling[10] and finite element micromechanical modelling[11] to approach and simulate human cochlear geometry, using the said mathematical models to describe the various parts of the cochlea in detail. Histological sectioning has been used to measure cochlear curvature, while liquid volume measurements have been used to assess cochlear volume.[12,13] The cochlear spiral has also been measured using orthogonal projection with computed tomography (CT) to reconstruct images of histological sections.[14] However, all the above experimental methods have been used on *in vitro* samples alone; none have included *in vivo* data.

The advancement of medical imaging techniques has led to the use of non-invasive modalities, CT and magnetic resonance imaging (MRI), for characterising anatomical geometry.[15–21] The development of 3D

Accepted for publication 27 May 2015 First published online 21 September 2015

reconstruction technology has allowed two-dimensional images to be rendered into 3D volume images.[22–24] These techniques have resulted in significant advances in inner-ear imaging.

The inherent nature of CT provides good *in vivo* delineation of bony anatomy in general, and the bony labyrinth in particular.[25] However, during cochlear implantation procedures, the electrode must pass the basal membrane of the membranous labyrinth, a soft tissue structure.[26,27] Therefore, MRI is arguably the optimum imaging modality with which to visualise and measure inner-ear anatomy, including any deformities. Thus, some researchers have opted to use MRI for inner-ear imaging. The modality has been used to aid surgeons in their clinical evaluation of the inner ear.[28] Another study used CT imaging to identify inner-ear deformities in patients with sensorineural hearing loss and investigate the deformities' role in hearing loss.[29] However, radiation is a concern when using CT imaging. Therefore, MRI could be an appropriate technology that enables reproducible findings in the measurement of the inner ear.

This study utilised MRI to non-invasively image the human bilateral cochlea *in vivo*. Image processing was used to obtain 3D volume images of right and left inner ears, and the bilateral cochlear spiral in particular. This was used to measure the length and curvature of each of the basal turn, middle turn and apex turn segments. These measurements provide an individual's geometry for pre-artificial cochlear implant assessment. The measurements can be used to plan the electrode insertion method and route, thus minimising potential damage by reducing the frictional, electrode recoil and adhesion forces during implantation.

Materials and methods

Cochlear imaging

A 3 T Magnetom Trio MRI scanner (Siemens, Erlangen, Germany) was used to acquire imaging data. The scanner produced images using a constructive interference in steady state ('CISS') gradient echo sequence, with a scanning repetition time and echo time of 5.65 ms and 2.6 ms respectively. Image data sets were comprised of 48 slices, with a pixel dimension of 0.5 mm × 0.5 mm × 0.5 mm.

Subjects

Eight human subjects (six male and two female) with no known inner-ear pathology were recruited. Four left inner ears and eight right inner ears were imaged.

The study was approved by the Institutional Review Board of Chang Gung Memorial Hospital (permit number: 99-1700B) and was conducted in accordance with the Declaration of Helsinki. Written informed consent was obtained from all subjects enrolled in the study.

Cochlear image processing

The length and curvature measurements will vary depending on the measurement location in the cochlear spiral. Thus, in order to standardise measurement, and obtain accurate and reproducible readings, the cochlear spiral volume image was manipulated and a fixed methodology was used to quantify the cochlear spiral length. The steps involved are described below.

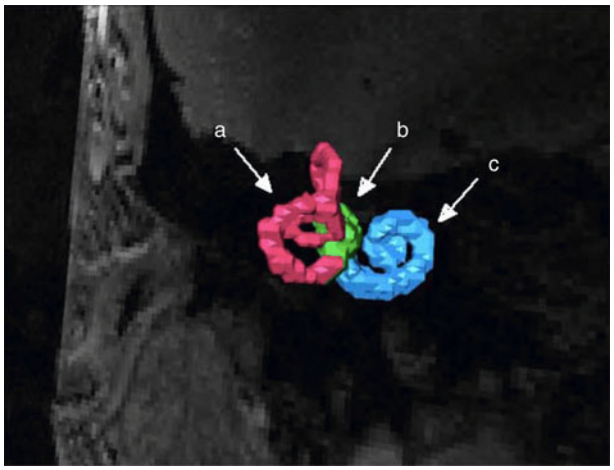

FIG. 1

A reconstructed, rendered three-dimensional image of the inner ear demonstrating: the semicircular canal ('a'), the ampullae ('b') and the cochlea ('c').

The images of the inner ear were threshold-adjusted to segment the image data corresponding to the inner ear. The data were subsequently reconstructed and rendered to generate a 3D image representing the inner ear, as demonstrated in Figure 1.

As electrode implantation requires insertion into the scala tympani, adjacent to the basal membrane of the membranous labyrinth, further image manipulation was required for this region.[26,27] The basal membrane was delineated from the scala tympani on the MRI image slices by eye, generating a further 3D volume representing the scala tympani.

In order to show the cochlear spiral path, the cochlea was displayed as a semi-transparent volume, represented by the outlined scala tympani, as shown in Figure 2.

The resulting spiral was then divided into three segments: the basal segment, the middle turn segment and

FIG. 2

A rendered three-dimensional, semi-transparent image of the cochlear spiral line (arrow).

https://doi.org/10.1017/S0022215115002480 Published online by Cambridge University Press

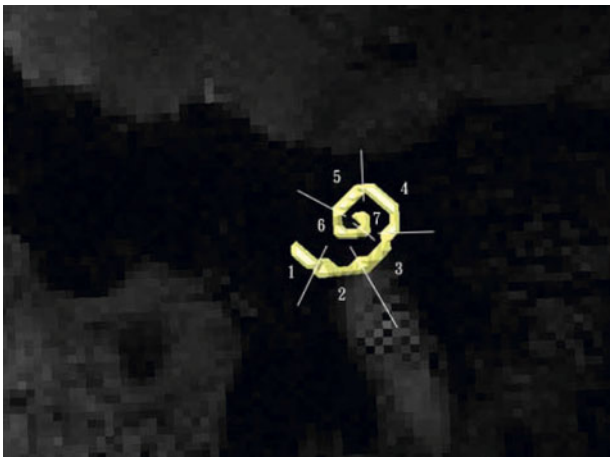

FIG. 3

Division of the cochlear spiral into base, middle and apex turn segments. The base and middle turn segments are subdivided into smaller segments. The segments are numbered thus: base turn segments (1–3), middle turn segment (4–6) and apex turn segment (7).

the apex turn segment. Two of the segments were subdivided as follows: those in the basal turn segment were numbered sections 1–3 and those in the middle turn segment were numbered sections 4–6. The apex turn segment was left undivided and numbered section 7, as shown in Figure 3.

Cochlear curvature measurements

Following division of the spiral into segments, the 3D co-ordinates of the mid and end points in each spiral segment (X_w, Y_w, Z_w) were identified, as shown in Figure 4, where the index 'w' denotes the point under consideration. The set of points are non-coplanar. A series of transformations were performed to place all points in a target plane.

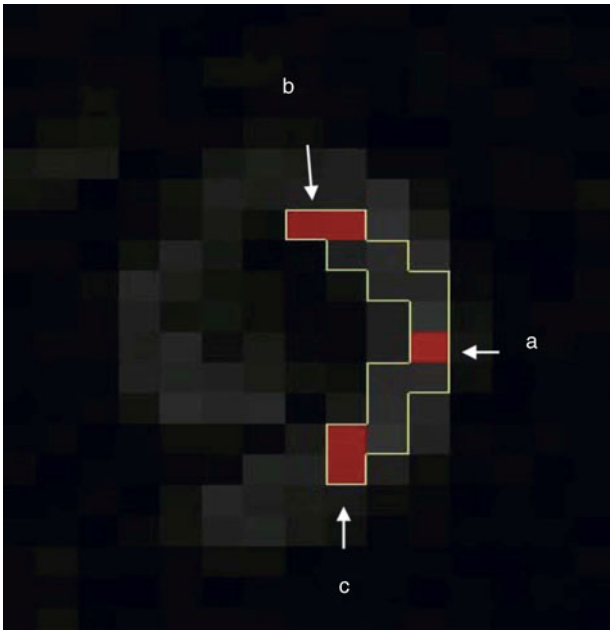

FIG. 4

Identification of the co-ordinates of the mid-point ('a') and end points ('b' and 'c') of each segment.

Firstly, using equation (1), (X_w, Y_w, Z_w) was transformed by (*tx, ty, tz*), to the new co-ordinates (X, Y, Z), holding the vector direction consistent. Note that 'T' is the transform function.

$$\begin{bmatrix} X \\ Y \\ Z \\ 1 \end{bmatrix} = T(-t_x, -t_y, -t_z) \cdot \begin{bmatrix} X_w \\ Y_w \\ Z_w \\ 1 \end{bmatrix} = \begin{bmatrix} 1 & 0 & 0 & -t_x \\ 0 & 1 & 0 & -t_y \\ 0 & 0 & 1 & -t_z \\ 0 & 0 & 0 & 1 \end{bmatrix} \cdot \begin{bmatrix} X_w \\ Y_w \\ Z_w \\ 1 \end{bmatrix} \quad (1)$$

Secondly, the points were rotationally transformed θ degrees about the X, Y, and Z axes using equations (2), (3) and (4) respectively.

$$\begin{bmatrix} X & Y & Z & 1 \end{bmatrix}^{\mathrm{T}} = R_z(-\theta) \cdot \begin{bmatrix} X_w & Y_w & Z_w & 1 \end{bmatrix}^{\mathrm{T}} = \begin{bmatrix} \cos\theta & \sin\theta & 0 & 0 \\ -\sin\theta & \cos\theta & 0 & 0 \\ 0 & 0 & 1 & 0 \\ 0 & 0 & 0 & 1 \end{bmatrix} \cdot \begin{bmatrix} X_w \\ Y_w \\ Z_w \\ 1_w \end{bmatrix} \quad (2)$$

$$\begin{bmatrix} X & Y & Z & 1 \end{bmatrix}^{\mathrm{T}} = R_x(-\theta) \cdot \begin{bmatrix} X_w & Y_w & Z_w & 1 \end{bmatrix}^{\mathrm{T}} = \begin{bmatrix} 1 & 0 & 0 & 0 \\ 0 & \cos\theta & \sin\theta & 0 \\ 0 & -\sin\theta & \cos\theta & 0 \\ 0 & 0 & 0 & 1 \end{bmatrix} \cdot \begin{bmatrix} X_w \\ Y_w \\ Z_w \\ 1 \end{bmatrix}$$

$$\begin{bmatrix} X & Y & Z & 1 \end{bmatrix}^{\mathrm{T}} = R_y(-\theta) \cdot \begin{bmatrix} X_w & Y_w & Y_w & 1 \end{bmatrix}^{\mathrm{T}} = \begin{bmatrix} \cos\theta & 0 & -\sin\theta & 0 \\ 0 & 1 & 0 & 0 \\ \sin\theta & 0 & \cos\theta & 0 \\ 0 & 0 & 0 & 1 \end{bmatrix} \cdot \begin{bmatrix} X_w \\ Y_w \\ Z_w \\ 1 \end{bmatrix}$$

The resulting target plane is shown in Figure 5.

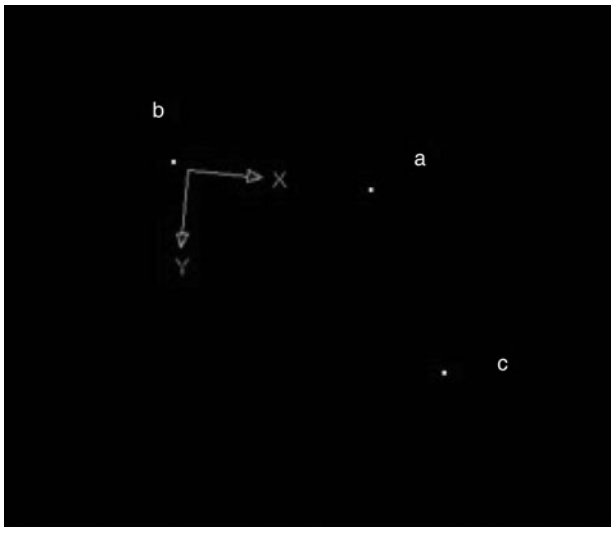

FIG. 5

Transformation of the non-coplanar mid-point ('a') and end point ('b' and 'c') co-ordinates into a target plane.

https://doi.org/10.1017/S0022215115002480 Published online by Cambridge University Press

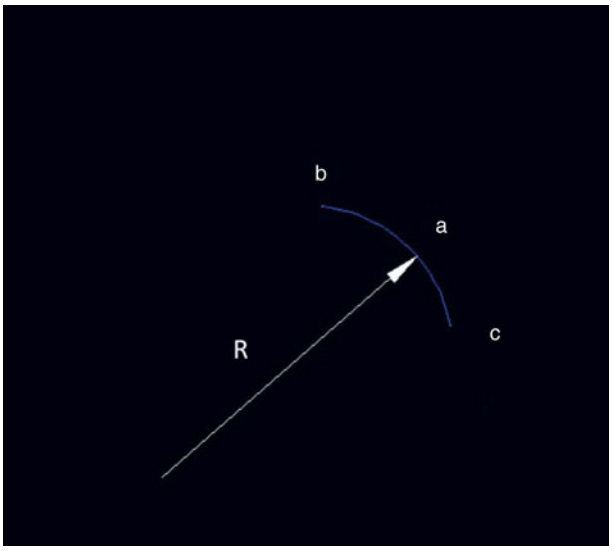

FIG. 6
The transformed target plane demonstrates mid-point ('a') and end points ('b' and 'c'), using AutoCAD software to calculate the curvature radius 'R'.

AutoCAD computer-aided design and drafting software (Autodesk, San Rafael, California, USA) was used to fit a curve between the three points in the target plane, the curvature of which was assumed to be the curvature of a given segment of the cochlea. AutoCAD was then used to measure the length and curvature radius, R, as shown in Figure 6. Curvature, ρ, is the inverse of curvature radius and was calculated using the formula $\rho = 1 / R$.

Results

Measurements of segment length and total cochlear length are demonstrated in Table I for the left cochlea and Table II for the right cochlea. The mean total left ear cochlear length was 3.11 cm (range, 2.81–3.55 cm). The mean total right ear cochlear length was 3.95 cm (range, 1.82–5.96 cm). This is in line with data in the literature.[30] For the left cochlea, the mean basal turn segment length was 1.35 cm (range, 0.85–2.03 cm), the mean middle turn segment length was 1.25 cm (range, 0.96–1.47 cm) and the mean apex turn segment length was 0.51 cm (range, 0.4–0.71 cm). For the right cochlea, the mean basal turn segment length was 1.55 cm (range, 0.68–2.52 cm), the mean middle turn segment was 1.83 cm (range, 0.95–3.39 cm), and the mean apex turn segment length was 0.57 cm (range, 0.19–1.02 cm).

In the left ear, the mean basal turn segment curvature was 3 cm^{-1} (range, 2.56–3.45 cm^{-1}), the mean middle turn segment curvature was 5.44 cm^{-1} (range, 4.55–6.67 cm^{-1}) and the mean apex turn segment curvature was 9.65 cm^{-1} (range, 6.67–12.5 cm^{-1}). In the right ear, the mean basal turn segment curvature was 2.5 cm^{-1} (range, 1.08–2.94 cm^{-1}), the mean middle turn segment curvature range was 4.41 cm^{-1} (range, 3.13–5.88 cm^{-1}) and the mean apex turn segment curvature was 10.09 cm^{-1} (range, 6.67–16.67 cm^{-1}).

TABLE I
LENGTH AND CURVATURE VALUES FOR LEFT BASE, MIDDLE AND APEX COCHLEAE

Inner-ear ID	Length (cm)			Total length (cm)	Curvature (1/cm)		
	Base	Middle	Apex		Base	Middle	Apex
1	1.52	0.96	0.42	2.9	3.45	6.67	12.5
2	2.03	1.12	0.4	3.55	2.56	4.55	8.33
3	0.85	1.47	0.49	2.81	3.03	5.26	11.11
4	0.99	1.46	0.71	3.16	2.94	5.26	6.67
Mean	1.35	1.25	0.51	3.11	3.00	5.44	9.65
SD	0.54	0.25	0.14	0.33	0.37	0.89	2.64

ID = identification; SD = standard deviation

TABLE II
LENGTH AND CURVATURE VALUES FOR RIGHT BASE, MIDDLE AND APEX COCHLEAE

Inner-ear ID	Length (cm)			Total length (cm)	Curvature (1/cm)		
	Base	Middle	Apex		Base	Middle	Apex
1	1	2.13	1.02	4.15	2.86	5.88	14.29
2	1.12	2.24	0.67	4.03	1.08	4.55	7.14
3	1.45	1.06	0.55	3.06	2.94	3.85	7.69
4	1.86	1.25	0.61	3.72	2.78	3.13	11.11
5	2.08	1.13	0.22	3.43	2.44	4.17	7.14
6	2.52	2.45	0.99	5.96	2.27	3.57	6.67
7	1.7	3.39	0.32	5.41	2.94	4.55	10
8	0.68	0.95	0.19	1.82	2.7	5.56	16.67
Mean	1.55	1.83	0.57	3.95	2.50	4.41	10.09
SD	0.61	0.87	0.32	1.30	0.62	0.94	3.72

ID = identification; SD = standard deviation

https://doi.org/10.1017/S0022215115002480 Published online by Cambridge University Press

Discussion

During an artificial cochlear implant procedure, the surgeons often have no prior knowledge of a patient's cochlear spiral anatomy. Thus, the force applied during insertion is largely a function of the surgeon's clinical acumen and experience, resulting in a potentially high risk of damage to the patient's scala tympani, with an associated risk of implant failure.[2] If a patient's cochlear spiral curvature measurements are obtained prior to the implantation procedure using medical imaging, surgeons may plan the optimum insertion track prior to the procedure, minimising excess force during insertion and reducing the risk of injury.

Measurements of right and left ears are compared in Figure 7. The mean total cochlear length is longer in the right ears examined, as are each of the individual cochlear segments. However, this difference does not reach statistical significance. Overall, the apex turn segment of the cochlea had the greatest degree of curvature for bilateral cochleae, as seen in Figure 8 ($p < 0.05$). The cochlear curvature was found to be greater in the basal and middle turn segments in the left ear compared to the right, while the apex turn segment's curvature was greater in the right ear compared to the left (Figure 8). These data highlight the differences that can exist in cochlear length and curvature between left and right cochleae.

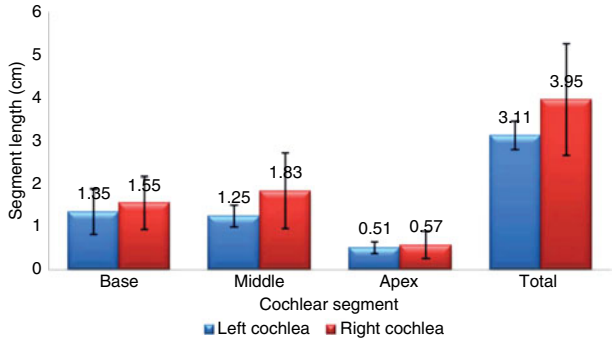

FIG. 7

Mean segment lengths and mean total lengths (with error bars) for the left and right cochleae.

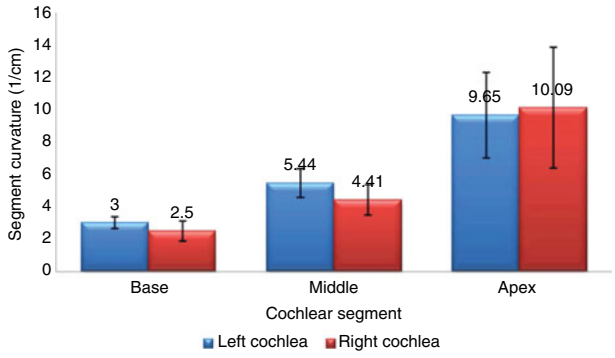

FIG. 8

Mean segment curvature measurements (with error bars) for the left and right cochleae.

- **This study quantified the geometric shape of the human inner-ear cochlea *in vivo***
- **Specifically, raw magnetic resonance imaging data were reconstructed to generate a three-dimensional image of the cochlea**
- **A detailed description of the cochlear spiral is provided, using curvature and length measurements**
- **Right cochleae mean total length was greater than left cochleae mean total length**
- **The data provide a valuable reference for cochlear implantation procedure development, to minimise potential implantation damage**

The data presented emphasise the need to describe each cochlea individually. It is hoped that the methodology described here will enable the provision of important anatomical information. Note that the head movement of subjects during the MRI scan will affect the imaging quality of the cochleae, which is a limitation of the present study. Furthermore, this methodology will allow pre-operative evaluation, and assessment of the electrode insertion technique and route, thus reducing the risk of damage to the cochlea. For bilateral cochleae, curvature changes can lead to excessive friction, pressure and adhesion forces in the apex turn segment during a cochlear implant procedure. The gradual increase in curvature, moving towards the apex turn segment, makes control of the electrode insertion position more difficult, highlighting the importance of an appreciation of cochlear length and curvature.

Conclusion

This study quantified the geometric shape of the human inner-ear cochlea *in vivo*, by reconstructing raw MRI data to generate a 3D image of the cochlea and its spirals. The spiral was separated into basal, middle and apex turn segments, and the lengths and curvatures of each section were measured. A comparison of left and right ears demonstrated that the right cochleae mean total length was greater than the left cochleae mean total length. Measurements showed greater curvature in the basal and middle turn segments of the left ear compared to the right ear, while the converse was true for the apex turn segment. On the basis of these results, in clinical terms, if bilateral artificial cochlear implants are required, each cochlea should be measured and assessed prior to surgery.

Pre-operative cochlear length and curvature measurements provide valuable information for surgeons, enabling them to evaluate the optimal electrode insertion method and route. This information increases

https://doi.org/10.1017/S0022215115002480 Published online by Cambridge University Press

insertion accuracy and reduces the risk of damage to the cochlea that may arise from excessive force. The data may also be used to improve and customise artificial cochlear design, such that the electrode adheres more closely to the basal membrane of the membranous labyrinth.

Acknowledgements

Support for this project was provided by Chang Gung Memorial Hospital (CMRPD190463). Facilities were provided by the Biomedical Engineering Center in Chang Gung University, Taiwan.

References

1 Skinner MW, Ketten DR, Holden LK, Harding GW, Smith PG, Gates GA *et al*. CT-derived estimation of cochlear morphology and electrode array position in relation to word recognition in Nucleus-22 recipients. *J Assoc Res Otolaryngol* 2002;**3**:332–50
2 Todd CA, Naghdy F, Svehla MJ. Force application during cochlear implant insertion: an analysis for improvement of surgeon technique. *IEEE Trans Biomed Eng* 2007;**54**:1247–55
3 Zrunek M, Burian K. Risk of basilar membrane perforation by intracochlear electrodes. *Arch Otorhinolaryngol* 1985;**242**: 295–9
4 Rebscher SJ, Heilmann M, Bruszewski W, Talbot NH, Snyder RL, Merzenich MM. Strategies to improve electrode positioning and safety in cochlear implants. *IEEE Trans Biomed Eng* 1999; **46**:340–52
5 Rebscher SJ, Talbot N, Bruszewski W, Heilmann M, Brasell J, Merzenich MM. A transparent model of the human scala tympani cavity. *J Neurosci Methods* 1996;**64**:105–14
6 Chen BK, Clark GM, Jones R. Evaluation of trajectories and contact pressures for the straight nucleus cochlear implant electrode array - a two-dimensional application of finite element analysis. *Med Eng Phys* 2003;**25**:141–7
7 Adunka O, Kiefer J, Unkelbach MH, Lehnert T, Gstoettner W. Development and evaluation of an improved cochlear implant electrode design for electric acoustic stimulation. *Laryngoscope* 2004;**114**:1237–41
8 Xu J, Briggs R, Tykocinski M, Newbold C, Risi F, Cowan R. Micro-focus fluoroscopy - a great tool for electrode development. *Cochlear Implants Int* 2009;**10**(suppl 1):115–19
9 Yoo SK, Wang G, Rubinstein JT, Vannier MW. Three-dimensional geometric modeling of the cochlea using helico-spiral approximation. *IEEE Trans Biomed Eng* 2000;**47**:1392–402
10 Vogel U. New approach for 3D imaging and geometry modeling of the human inner ear. *ORL J Otorhinolaryngol Relat Spec* 1999;**61**:259–67
11 Kolston PJ, Ashmore JF. Finite element micromechanical modeling of the cochlea in three dimensions. *J Acoust Soc Am* 1996; **99**:455–67
12 Saito R, Igarashi M, Alford BR, Guilford FR. Anatomical measurement of the sinus tympani. A study of horizontal serial sections of the human temporal bone. *Arch Otolaryngol* 1971; **94**:418–25
13 Xiang Z-Y, Zhao X-S, Xiao S-K, Luo L-P, Wei R-Y, Zhao L-R. Experimental study of the accuracy of Siemens Sensation 4 volume software [in Chinese]. *Chinese Journal of Medical Imaging Technology* 2003;**19**:1223–4
14 Manoussaki D, Chadwick RS, Ketten DR, Arruda J, Dimitriadis EK, O'Malley JT. The influence of cochlear shape on low-frequency hearing. *Proc Natl Acad Sci U S A* 2008;**105**:6162–6
15 Purcell DD, Fischbein NJ, Patel A, Johnson J, Lalwani AK. Two temporal bone computed tomography measurements increase recognition of malformations and predict sensorineural hearing loss. *Laryngoscope* 2006;**116**:1439–46
16 Ozgen B, Cunnane ME, Caruso PA, Curtin HD. Comparison of 45 degrees oblique reformats with axial reformats in CT evaluation of the vestibular aqueduct. *AJNR Am J Neuroradiol* 2008; **29**:30–4
17 Tanioka H, Kaga H, Zusho H, Araki T, Sasaki Y. MR of the endolymphatic duct and sac: findings in Meniere disease. *AJNR Am J Neuroradiol* 1997;**18**:45–51
18 Niyazov DM, Andrews JC, Strelioff D, Sinha S, Lufkin R. Diagnosis of endolymphatic hydrops in vivo with magnetic resonance imaging. *Otol Neurotol* 2001;**22**:813–17
19 Nakashima T, Naganawa S, Sugiura M, Teranishi M, Sone M, Hayashi H *et al*. Visualization of endolymphatic hydrops in patients with Meniere's disease. *Laryngoscope* 2007;**117**: 415–20
20 Hsieh M-S, Lee F-P, Tsai M-D. A virtual reality ear ossicle surgery simulator using three-dimensional computer tomography. *J Med Biol Eng* 2010;**30**:57–63
21 Chen Y-S, Chen L-F, Chang Y-T, Huang Y-T, Su T-P, Hsieh J-C. Quantitative evaluation of brain magnetic resonance images using voxel-based morphometry and Bayesian theorem for patients with bipolar disorder. *J Med Biol Eng* 2008;**28**:127–33
22 Morita N, Kariya S, Farajzadeh Deroee A, Cureoglu S, Nomiya S, Nomiya R *et al*. Membranous labyrinth volumes in normal ears and Meniere disease: a three-dimensional reconstruction study. *Laryngoscope* 2009;**119**:2216–20
23 Teranishi M, Yoshida T, Katayama N, Hayashi H, Otake H, Nakata S *et al*. 3D computerized model of endolymphatic hydrops from specimens of temporal bone. *Acta Otolaryngol Suppl* 2009;(560):43–7
24 Migueis A, Melo Freitas P, Cordeiro M. Anatomic evaluation of the membranous labyrinth by imaging: 3D-MRI volume-rendered reconstructions. *Rev Laryngol Otol Rhinol (Bord)* 2007;**128**:37–40
25 Tomandl BF, Hastreiter P, Eberhardt KE, Rezk-Salama C, Naraghi R, Greess H *et al*. Virtual labyrinthoscopy: visualization of the inner ear with interactive direct volume rendering. *Radiographics* 2000;**20**:547–58
26 Kha HN, Chen BK, Clark GM. 3D finite element analyses of insertion of the Nucleus standard straight and the Contour electrode arrays into the human cochlea. *J Biomech* 2007; **40**:2796–805
27 Hanekom T. Three-dimensional spiraling finite element model of the electrically stimulated cochlea. *Ear Hear* 2001;**22**: 300–15
28 Lane JI, Ward H, Witte RJ, Bernstein MA, Driscoll CL. 3-T imaging of the cochlear nerve and labyrinth in cochlear-implant candidates: 3D fast recovery fast spin-echo versus 3D constructive interference in the steady state techniques. *AJNR Am J Neuroradiol* 2004;**25**:618–22
29 Chen JL, Gittleman A, Barnes PD, Chang KW. Utility of temporal bone computed tomographic measurements in the evaluation of inner ear malformations. *Arch Otolaryngol Head Neck Surg* 2008;**134**:50–6
30 Yost WA. *Fundamentals of Hearing: An Introduction*, 4th edn. San Diego: Academic Press, 2000

Address for correspondence:
Dr Jen-Fang Yu,
Graduate Institute of Medical Mechatronics,
Chang Gung University,
259 Wen-Hwa 1st Road,
Kwei-Shan 333,
Taoyuan, Taiwan

Fax: +886 3 2118050
E-mail: jfyu.phd@gmail.com

Dr J-F Yu takes responsibility for the integrity of the content of the paper
Competing interests: None declared